Joule

CellPress

Article

Microchannel-elevated micromembrane for sustainable phase-separation condensation

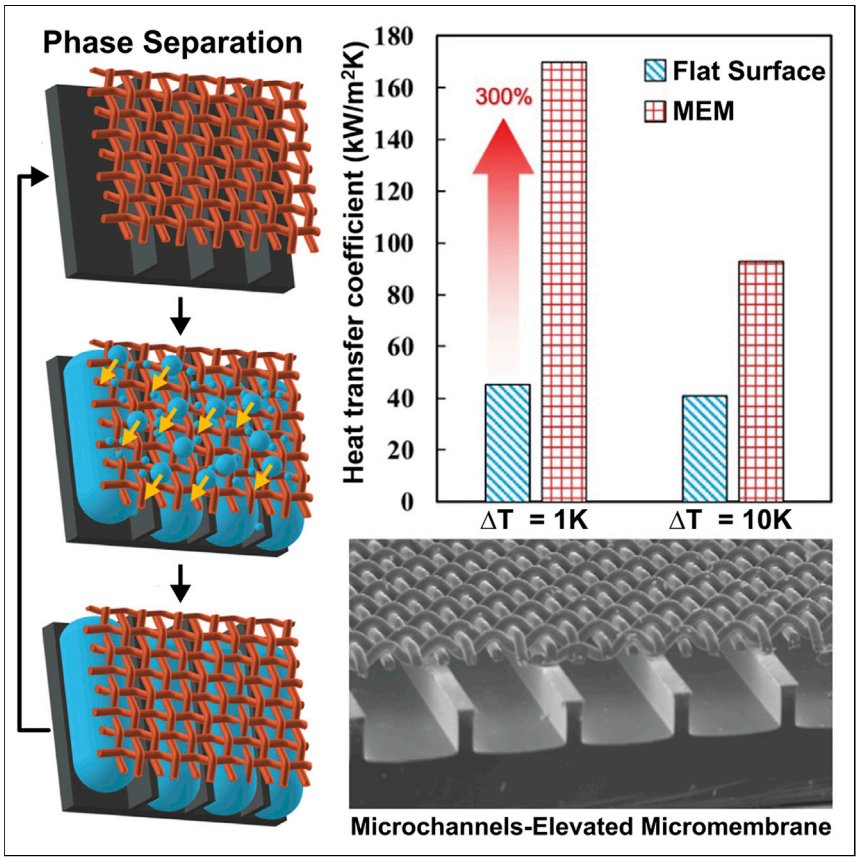

We achieved phase-separation condensation on the microchannel-elevated micromembrane (MEM) with a hydrophobic micromembrane for vapor-liquid flow separation and slippery microchannels for condensate removal to prevent flooding. The phase-separation condensation on MEM shows a heat transfer coefficient 300% higher than that of the dropwise condensation on a hydrophobic flat surface. Moreover, it sustains phase separation at a heat flux of 1,000 kW/m^2 without apparent failure.

Li Shan, Zongqi Guo, Deepak Monga, Dylan Boylan, Xianming Dai

dai@utdallas.edu

Highlights

Phase separation promotes heat transfer by 300% compared with dropwise condensation

Hydrophobic micromembrane separates vapor and liquid flow

Slippery microchannel aids in rapid droplet removal and sustainable phase separation

High heat transfer coefficient is sustained at a heat flux of 1,000 kW/m^2

Shan et al., Joule 7, 1–15
January 18, 2023
https://doi.org/10.1016/j.joule.2022.11.010

Please cite this article in press as: Shan et al., Microchannel-elevated micromembrane for sustainable phase-separation condensation, Joule (2022), https://doi.org/10.1016/j.joule.2022.11.010

Joule

CellPress

Article

Microchannel-elevated micromembrane for sustainable phase-separation condensation

Li Shan,[1,2] Zongqi Guo,[1,2] Deepak Monga,[1] Dylan Boylan,[1] and Xianming Dai[1,3,*]

SUMMARY

A sustainable high heat transfer coefficient is critical for water and energy systems that utilize steam condensation. Current techniques cannot achieve a high heat transfer performance at a high heat flux. It is desired to separate vapor and liquid flow to provide a large surface area for condensation. Here, we report sustainable phase separation on microchannel-elevated micromembrane (MEM) by (1) separating the vapor and liquid using a hydrophobic micromembrane that rapidly removes condensed droplets to achieve a high heat transfer coefficient and (2) sustaining continual condensate removal inside the hydrophobic microchannels beneath the micromembrane to prevent flooding. We found that MEM could sustain phase separation at a heat flux of 1,000 kW/m^2 without apparent failure. The heat transfer coefficient is 300% higher than that of the dropwise condensation on a hydrophobic flat surface. The phase separation on MEM provides a paradigm for sustainable high-performance condensation regardless of subcooling.

INTRODUCTION

Condensation of steam is a critical process in water and thermal energy systems, including atmospheric water harvesting,[1–3] seawater desalination,[4] thermal management of electronics,[5,6] heat exchangers,[7,8] and thermal energy systems.[8,9] Phase change heat transfer in steam condensation utilizes the large latent heat, which can achieve high heat transfer performance and enhance the overall energy saving. Generally, steam condensation has two modes: filmwise condensation and dropwise condensation. In filmwise condensation, a wettable surface is covered by a thick liquid film, which acts as a thermal barrier and reduces the heat transfer coefficient (HTC).[10,11] In dropwise condensation, droplets nucleate on the non-wettable surfaces and shed as discrete droplets. This significantly reduces the thermal resistance, leading to an order of magnitude higher HTC than that of filmwise condensation.[12] However, the condensed small droplets are hard to remove. They need to grow and coalesce with each other to reach a shedding diameter, so that the gravitational force can overcome the pinning force to remove condensates.[13,14] From droplet nucleation to its complete removal from the condensing surface, it is always a thermal barrier for further steam condensation. A report from the US Department of Energy shows the steam heating system is often used in multifamily housing units.[15] If the condensation HTC on the steam radiator is improved by 300%, the overall system heat transfer performance is increased by 13%, which can save energy and cost for the steam heating system.[15–17]

To achieve a high condensation performance, surfaces must remove droplets from the surface immediately as they nucleate. This minimizes the thermal resistance and provides a droplet-free surface for rapid re-nucleation. Quasi-liquid surfaces

CONTEXT & SCALE

Condensation is a ubiquitous vapor-to-liquid-phase-change phenomenon in water and energy systems. The heat transfer coefficient is a key parameter to characterize the condensation performance, which typically decreases with an increased subcooling due to the partial flooding at elevated heat fluxes. However, steam power plants and refrigeration systems operate at a large subcooling that leads to a poor heat transfer performance due to flooding. Here, we introduce a previously unachieved approach that uses microchannel-elevated micromembrane to separate vapor and liquid on the top micromembrane and remove condensed liquids through the bottom microchannels. The vapor-liquid separation provides a large area for condensation without flooding. As a result, a sustainable high heat transfer coefficient is achieved at varying heat fluxes.

(QLS)[14] and slippery liquid-infused porous surfaces (SLIPS)[18] with active oil replenishing can reduce the surface pinning force and provide a smaller droplet removal diameter of less than 1 mm, which leads to a fast surface refreshing rate and reduces the overall thermal resistance. However, the droplet removal size is still too large to achieve a high HTC. Then, flat surfaces with patterned wettability were used to separate droplet nucleation and removal.[19–24] Periodic hydrophilic and hydrophobic strip patterns on these surfaces result in simultaneous filmwise and dropwise condensation. When droplets grow in the hydrophobic area, they are absorbed into the liquid film in the hydrophilic area. Although part of the surfaces is covered with thick liquid films, the rapid droplet removal results in an 18% enhancement in HTC at a lower subcooling compared with that of dropwise condensation.[25] However, the HTC decreases significantly with the subcooling due to surface flooding as condensation rates increase at elevated heat fluxes. To further enhance the heat transfer performance and delay surface flooding, microchannels were investigated by researchers due to their large specific surface area for nucleation and large droplet removal frequency. The microchannels have enhanced droplet removal by liquid imbibition.[26] However, they are covered by large droplets at an elevated heat flux, which undermines the heat transfer performance.[27] Afterward, superhydrophobic surfaces with micro/nanoscale structures were developed for jumping-droplet condensation.[28–31] When small droplets coalesce on superhydrophobic surfaces, they jump from the surfaces due to the release of surface energy during coalescence, so the droplet removal diameter and the overall thermal resistance on the surface are reduced.[32] Thus, a 60% higher HTC than that of the conventional shedding-droplet condensation is achieved.[33] However, the jumping-droplet condensation inevitably transitions from dropwise to filmwise condensation because nanoscale droplets nucleate within the superhydrophobic structures, which leads to a sharp decrease in the HTC as a function of subcooling. To delay the transition, three-dimensional (3D) hybrid surfaces with patterned superhydrophobic surfaces and hydrophilic microchannels were used to promote droplet removal.[34] Nevertheless, flooding is inevitable on hybrid surfaces due to the flooding of hydrophilic microchannels at elevated heat fluxes. Furthermore, hydrophilic porous structures were designed to rapidly remove the top condensed droplets at a small diameter.[35–37] As small droplets nucleate and grow on the porous structure surface, they are absorbed into the pores at a diameter of 50 μm.[36] The rapid removal of droplets on these surfaces provided a 100% higher HTC than that on hydrophobic flat surfaces. Due to the liquid imbibition in the porous structures, the inner pores are filled with condensate, leading to gradual flooding. Researchers also tried to confine a thin liquid film in 3D condensation structures for rapid droplet absorption at smaller diameters, such as the copper inverse opal structures,[36] and amphiphilic micropillars.[37] In addition, liquid suction behavior generated by wettability gradients on a 3D structure was used to promote liquid removal from condensing surfaces.[38] However, the porous structures suffer from a large pinning force and high flow resistance, which made the liquid trapped in pores hard to be removed by gravitational force. As the subcooling increases, the condensed liquid would expand out from the pores and form large droplets on the surface. Eventually, the HTC became the same as that of filmwise condensation due to surface flooding. On these state-of-the-art condensation surfaces, a high HTC can be achieved by rapidly removing condensed droplets and increasing the surface areas. However, a sharp decrease in HTC is always observed due to the limitation of liquid removal, which leads to poor sustainability with increased subcooling.

To address these challenges, we have designed microchannel-elevated micromembrane (MEM) that can achieve sustainable phase-separation condensation up to a

[1]Department of Mechanical Engineering, University of Texas at Dallas, Richardson, TX 75080, USA

[2]These authors contributed equally

[3]Lead contact

*Correspondence: dai@utdallas.edu

https://doi.org/10.1016/j.joule.2022.11.010

Please cite this article in press as: Shan et al., Microchannel-elevated micromembrane for sustainable phase-separation condensation, Joule (2022), https://doi.org/10.1016/j.joule.2022.11.010

high subcooling. The MEM structure consists of a hydrophobic mesh membrane as the condensing surface and hydrophobic microchannels for sustainable rapid liquid removal. The liquid columns are formed in the microchannels due to droplet nucleation, growth, and coalescence. As each liquid column grows and contacts the hydrophobic mesh, the condensed droplets on the mesh membrane are removed, which separates the vapor and liquid flow. Furthermore, the small flow resistances of microchannels result in the rapid removal of liquid columns without apparent flooding. Phase-separation condensation on MEM can rapidly remove condensed droplets to refresh the surface for nucleation, leading to a higher HTC. We found that MEM could sustain phase separation at a heat flux of 1,000 kW/m^2 at a subcooling of 10 K without apparent failure, while a hydrophobic flat surface can only reach 400 kW/m^2. We achieved a maximum HTC of 170 kW/m^{2}K, which is 300% higher than that of the dropwise condensation on a hydrophobic flat surface with an HTC of 43 kW/m^{2}K. Compared with the state-of-the-art surfaces that have been developed to enhance condensation, MEM does not need sticky hydrophilic domains to remove droplets so it can significantly delay flooding at an elevated subcooling (Table S1). In addition, MEM uses commercially available copper woven mesh, which leads to simple and cost-effective fabrications.

RESULTS AND DISCUSSION

Design rationale of MEM for phase separation

To achieve a sustainable high HTC, there are two design criteria. (1) To achieve a high HTC, the nucleated droplets must be rapidly removed from the condensing surface to reduce thermal resistance. In addition, there must be a large effective surface area for droplet nucleation. (2) To sustain a high HTC with increased subcooling, surface flooding must be avoided at elevated subcooling. To satisfy the design criteria, separating vapor and liquid flow is highly desirable as it can minimize the contact between vapor and liquid. Thus, vapor can be directly condensed on the liquid-free surface to maximize the heat transfer performance.

First, we show the design of MEM for its phase-separation condensation. Second, we experimentally investigated the steam condensation on MEM and state-of-the-art surfaces, including a hydrophobic flat surface (baseline) and a two-layer mesh surface at varying subcooling. Third, we investigated the design criteria of microchannel sizes to achieve phase-separation condensation on MEM. Fourth, quasi-liquid coatings and two-layer meshes are used to further increase the HTC on MEM. Our experimental results show that the phase-separation condensation on hydrophobic MEM provides sustainable high HTC regardless of subcooling due to the rapid liquid removal. A MEM with two-layer meshes achieves a maximum HTC of 170 kW/m^{2}K, which is 300% higher than that on the baseline surface with an HTC of 43 kW/m^{2}K.

To achieve a sustainable high HTC with increased subcooling, we developed a phase-separation condensation mode to separate vapor and liquid flow in steam condensation on a newly developed MEM surface. We fabricated MEM with a copper mesh bonded on microchannels through electroplating (Figures 1A–1C), see detail in experimental procedures). We used microchannels as the base structure of MEM for liquid removal because of its small pinning force compared with other structures, such as micropillars (Figure S1; Note S1). A mesh with a wire diameter of 50 μm and an inter-mesh spacing of 50 μm is used in this study. With the increase in wire diameter, the maximum droplet removal diameter becomes larger, which leads to a larger thermal resistance and a lower refreshing frequency (Figure S2; Note S2). The entire MEM was coated with silane. The mesh offers a large surface

Please cite this article in press as: Shan et al., Microchannel-elevated micromembrane for sustainable phase-separation condensation, Joule (2022), https://doi.org/10.1016/j.joule.2022.11.010

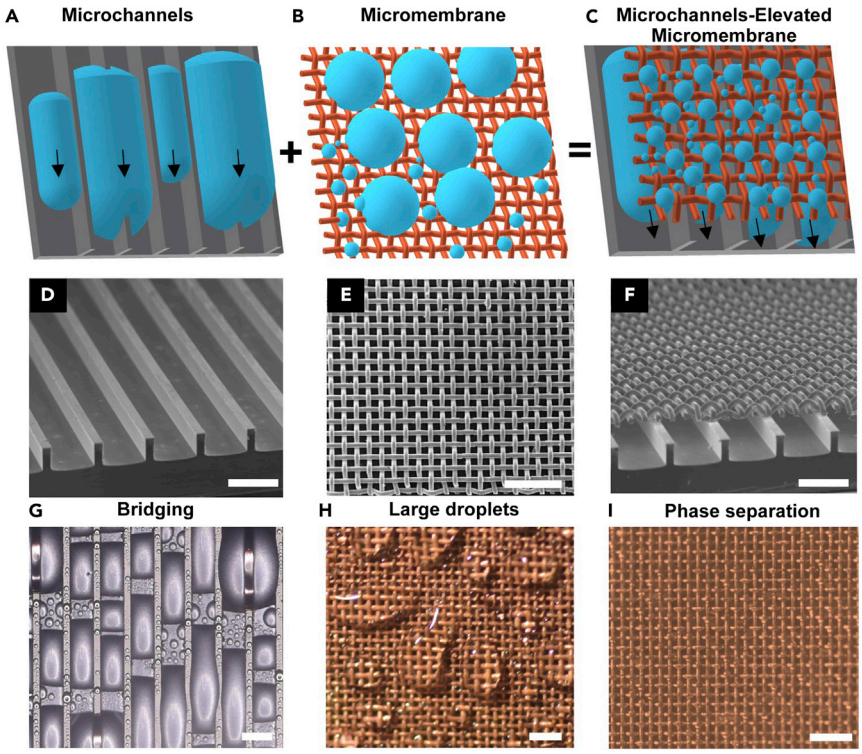

Figure 1. Design rationale of microchannel-elevated micromembrane to achieve phase-separation condensation

(A–C) Schematic drawings for the condensation on three hydrophobic surfaces, i.e., (A) microchannels, (B) micromembrane, and (C) MEM. Elongated liquid columns formed inside the microchannels and shed off quickly as some bridge over the microchannels walls. On the hydrophobic micromembrane, the condensed droplets grow, coalesce, and form large droplets. When the microchannels are combined with the micromembrane, liquid columns that are confined in the microchannels rapidly absorb nucleated droplets on the micromembrane and shed off due to the gravitational force.

(D–F) SEM images of hydrophobic (D) microchannels, (E) micromembrane, and (F) MEM.

(G–I) Experimental images for steam condensation on the hydrophobic (G) microchannels, (H) micromembrane, and (I) MEM. There are no obvious droplets on MEM due to phase separation. The scale bars are 500 μm for all.

area for nucleation, while the pores on the mesh provide a pathway for droplet removal. Moreover, hydrophobic microchannels enable rapid liquid shedding by gravitational force to prevent flooding on the condensation surface at a large subcooling.

Then, we experimentally investigated the phase-separation condensation on MEM in a custom-built steam chamber (see detail in experimental procedures). We investigated the condensation behaviors on three hydrophobic surfaces, i.e., microchannels (Figure 1D), micromembrane (Figure 1E), and MEM (Figure 1F). The hydrophobic microchannels show that the condensed liquid forms an elongated liquid column and moves along the microchannels (Figure 1G). The top of the microchannels is not confined, so multiple liquid columns coalesce over the microchannel walls and shed off as large droplets. On a hydrophobic micromembrane, nucleated droplets grow and coalesce on the top of the micromembrane and form large droplets, which act as thermal barriers (Figure 1H). As we combine the microchannels with the micromembrane to form hydrophobic MEM, the small droplets on the micromembrane were rapidly absorbed into the microchannels by the liquid columns

Please cite this article in press as: Shan et al., Microchannel-elevated micromembrane for sustainable phase-separation condensation, Joule (2022), https://doi.org/10.1016/j.joule.2022.11.010

(Figure 1I), which can shed off spontaneously due to the low flow resistance. The combination of micromembrane and microchannels provides a larger nucleation area and rapid condensate removal, which leads to a sustainable phase-separation condensation on MEM.

Phase-separation condensation enabled by liquid columns in microchannels

To elucidate the phase-separation process on the MEM, we studied the condensate removal mechanism on MEM, which have a microchannel width of 400 μm, named MEM-400. If not specified, the hydrophobic mesh used in this work has a wire diameter of 50 μm and an inter-mesh spacing of 50 μm, and all MEM reported in this paper have a channel depth of 200 μm and a wall width of 100 μm. We used the hydrophobic flat surface as the baseline for all our studies. Figure 2A shows the schematics of the condensation mechanism on MEM-400. Small droplets form in the microchannels and on the mesh at the nucleation stage. As droplets in the microchannels grow and coalesce, they turn into elongated liquid columns due to the confinement of the mesh and the microchannel sidewalls. The droplets on the mesh are absorbed into the channels immediately once they contact the liquid columns. As more condensed droplets are absorbed into the microchannels, the liquid columns grow in length and volume. This results in the shedding of the liquid columns and refreshing on the MEM. Figure 2B shows the microscopic images of the liquid removal on the mesh of MEM-400. The rapid removal of droplets above 50 μm enables the rapid refreshing of the mesh and leads to effective phase separation (Video S1). As a comparison, we studied the condensation behavior of the two-layer hydrophobic meshes (Figures 2C and 2D), which were one of state-of-the-art surfaces used previously in steam condensation.[39] The hydrophobic two-layer meshes coated flat substrate could also achieve phase separation with small droplets on the mesh surface (Figure S3). However, it can only be sustained at a low subcooling ($\Delta T < 4$ K). When the subcooling is increased, flooding occurs on the surface (Figures 2C and 2E). Due to the water storage and the large pinning force of the porous structure, condensates form a thick liquid film in the structures. Eventually, the condensate expands out from the pores of the mesh and forms large droplets on the mesh surface which results in flooding (Figure 2D).

Furthermore, we measured the HTC of MEM-400 and compared it with the hydrophobic two-layer meshes, and the hydrophobic flat surface as shown in Figure 2E. The two-layer meshes show a comparable HTC with MEM-400 at a subcooling of 1 K, which is 170% higher than the hydrophobic flat surface due to its large surface area and smaller thermal resistance. However, the HTC on the two-layer mesh sharply decreases with the increased subcooling because the large flow resistance through the small pores hinders the bulk liquid removal, leading to surface flooding (Figure S3). At the subcooling of 10 K, MEM-400 shows a sustainable phase separation with an HTC of 72 kW/m^{2}K, which is a heat transfer enhancement of up to 80% compared with two-layer meshes due to the efficient phase separation. We also experimentally investigated the heat transfer performance of MEM with the presence of non-condensable gases and at an elevated pressure of 20 kPa, respectively. The HTCs were significantly higher on MEM than those on hydrophobic flat surfaces in both conditions (Figure S4).

To gain more insight into the failure mechanism of two-layer meshes and the sustainable phase separation of MEM-400, we used the Ergun equation[40–42] to evaluate the flow resistance as a function of heat flux (Figure 2F; Note S3). To remove the condensate continuously, the flow resistance must be smaller than the hydrostatic pressure of 200 Pa for a 2 mm sample length, provided by the gravitational force. The mass

Please cite this article in press as: Shan et al., Microchannel-elevated micromembrane for sustainable phase-separation condensation, Joule (2022), https://doi.org/10.1016/j.joule.2022.11.010

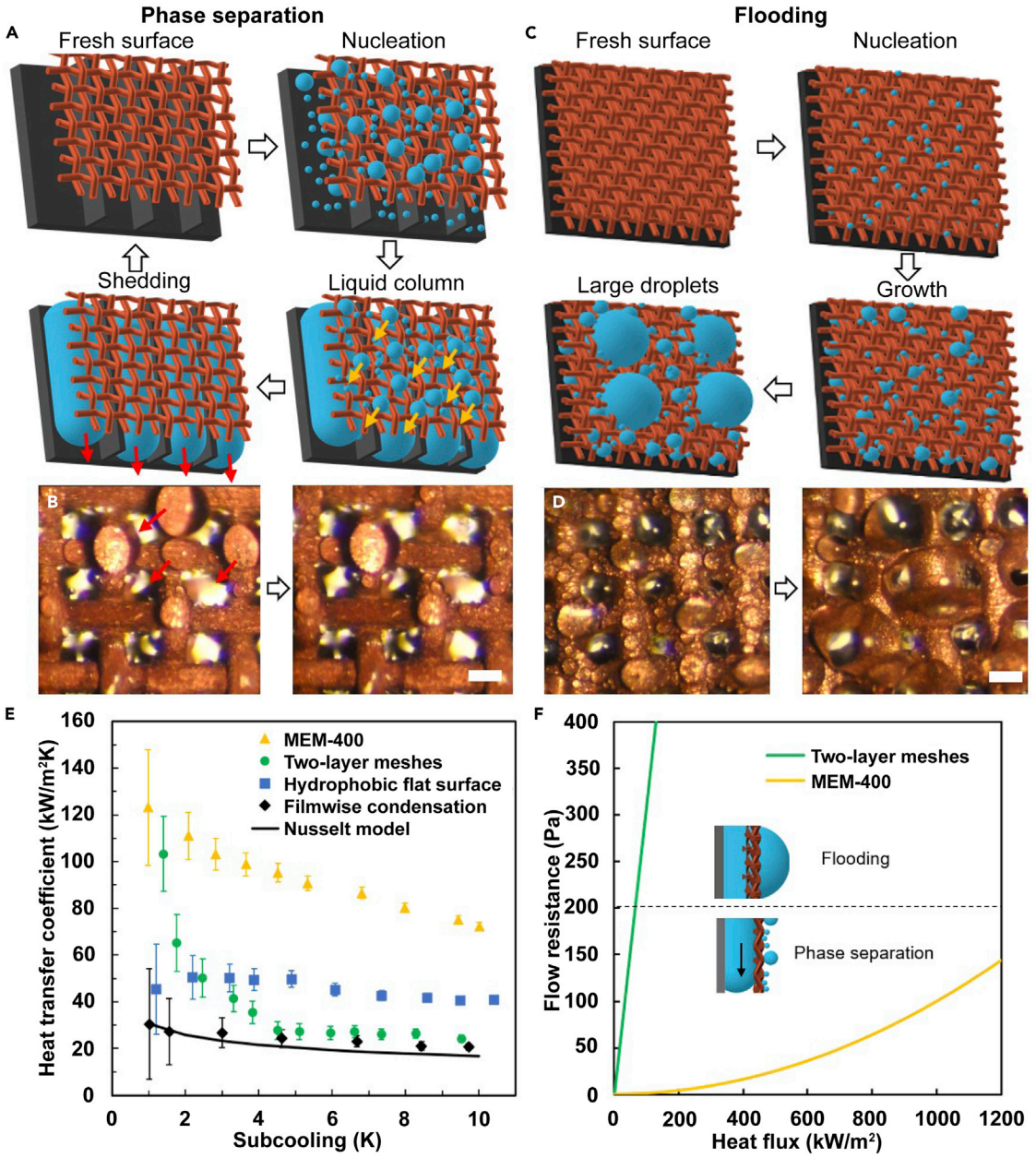

Figure 2. A sustainable high-performance condensation achieved by phase separation using MEM

(A) Schematics show the condensation behavior on MEM. Condensed droplets are rapidly removed from the mesh and absorbed in the microchannels due to the contact with liquid columns. Liquid columns are rapidly removed due to the small flow resistance.

(B) Microscopic views of the condensation behavior on the mesh of MEM. Nucleated droplets are rapidly absorbed into the microchannels through mesh pores. Scale bars, 50 μm.

(C) Schematics show the condensation behavior on two-layer meshes that are bonded on a flat substrate. Large flow resistance hinders the removal of liquid film and condensate expands out from the mesh pores, leading to surface flooding.

(D) Microscopic views of the condensation behavior on the two-layer meshes. Liquid pops out from the mesh pores. Scale bars, 50 μm.

(E) Experimental heat transfer coefficient for MEM-400, two-layer meshes on a flat surface, and hydrophobic flat surface as a function of subcooling.

(F) Theoretical calculation of flow resistance for MEM-400 and two-layer meshes on a flat surface as a function of the heat fluxes. Two-layer mesh structure showed a high flow resistance at an elevated heat flux, leading to surface flooding. The microchannels of MEM provide a low flow resistance, which delays the transition from phase separation to flooding.

Please cite this article in press as: Shan et al., Microchannel-elevated micromembrane for sustainable phase-separation condensation, Joule (2022), https://doi.org/10.1016/j.joule.2022.11.010

flow rate is small at low heat flux conditions and condensate can be efficiently removed from the surface for both the two-layer meshes and MEM-400. However, the flow resistance for two-layer meshes increases significantly with the increasing heat flux. The condensed liquid cannot be removed from the porous structures, and the surface becomes flooded. The two-layer meshes can only achieve a rapid phase separation at extremely low heat fluxes up to 60 kW/m^2. The microchannels of MEM-400 offer small flow resistances due to the large cross-sectional area of the microchannels. Thus, MEM shows sustainable phase separation at an elevated heat flux of 1,000 kW/m^2. Therefore, a sustainable high HTC with increased subcooling is achieved by MEM due to the effective phase separation.

Designing the microchannels of MEM

We characterized the condensation behavior of MEM with three channel widths (W_c): 200, 400, and 800 μm, named MEM-200, MEM-400, and MEM-800, respectively (Figures 3A–3C). On a hydrophobic flat surface, the shedding diameter is 650 μm.[14] The elongated liquid columns form in the microchannels due to the confinement of the top hydrophobic mesh and the microchannel sidewalls when $0 < W_c < 650$ μm. Particularly, the flow resistance is small as $W_c > 300$ μm. When $W_c \geq 650$ μm, condensate sheds as discrete droplets in the channels. All experiments were performed with vertically mounted samples with an inclination angle of 90°. Surfaces with an inclination angle of 45° were tested, and the heat transfer enhancements remained large (Figure S5; Note S3). To visualize the condensation behavior both in the slippery microchannels and on the hydrophobic mesh, the mesh is partially covered on the microchannels. The experiments were carried out on hydrophobic MEM in a closed steam condensation chamber operating at a relative pressure of 6.9 kPa (see experimental procedures for details). (1) At a subcooling of 1 K, MEM-200 and MEM-400 both show phase separation with small droplets on the hydrophobic mesh (Figure S6). Since their channel widths are smaller than the shedding diameter of droplets on a flat surface (650 μm),[14] the elongated liquid columns form in the microchannels due to the confinement of the top hydrophobic mesh and the microchannel sidewalls. As the droplets nucleate and grow on the hydrophobic mesh, they contact the liquid columns, leading to droplet absorption from the mesh to the microchannels and leaving a fresh mesh surface for further condensation. The liquid columns grow longer as more droplets are absorbed into the microchannels and shed off due to gravitational force when they reach a critical length. (2) At a subcooling of 5 K, the liquid columns in the microchannels of MEM-200 start to pop out from the pores of the mesh, giving rise to a flooded liquid film as shown in Figures 3A and 3D and Video S2. (3) At a subcooling of 10 K, the MEM-400 still shows a sustainable phase-separation performance with continuous shedding of liquid columns in the microchannels (Figures 3B and 3E; Video S2). As the channel sizes are larger than the shedding diameter of the droplet on a flat surface ($W_c > 650$ μm), droplets shed off in the microchannel without touching the nucleated droplets on the micromembrane, such as the shedding droplets on MEM-800 (Figures 3C and 3F; Video S2). Therefore, the condensed droplets on the hydrophobic mesh coalesce and form large droplets, which act as thermal barriers for further condensation.

We experimentally measured the HTC of MEM-200, MEM-400, and MEM-800 at different subcooling. At a subcooling of 1 K, MEM-200 shows the highest HTC of 134 kW/m^{2}K due to the large specific surface area provided by the mesh and channels (Figure 3G). However, the HTC decreases sharply with the increased subcooling due to the flooding in the microchannels, eventually leading to the filmwise condensation at a subcooling above 5 K. In contrast, MEM-400 shows a sustainable high HTC at elevated subcooling. At a subcooling of 10 K, MEM-400 shows a high HTC

Please cite this article in press as: Shan et al., Microchannel-elevated micromembrane for sustainable phase-separation condensation, Joule (2022), https://doi.org/10.1016/j.joule.2022.11.010

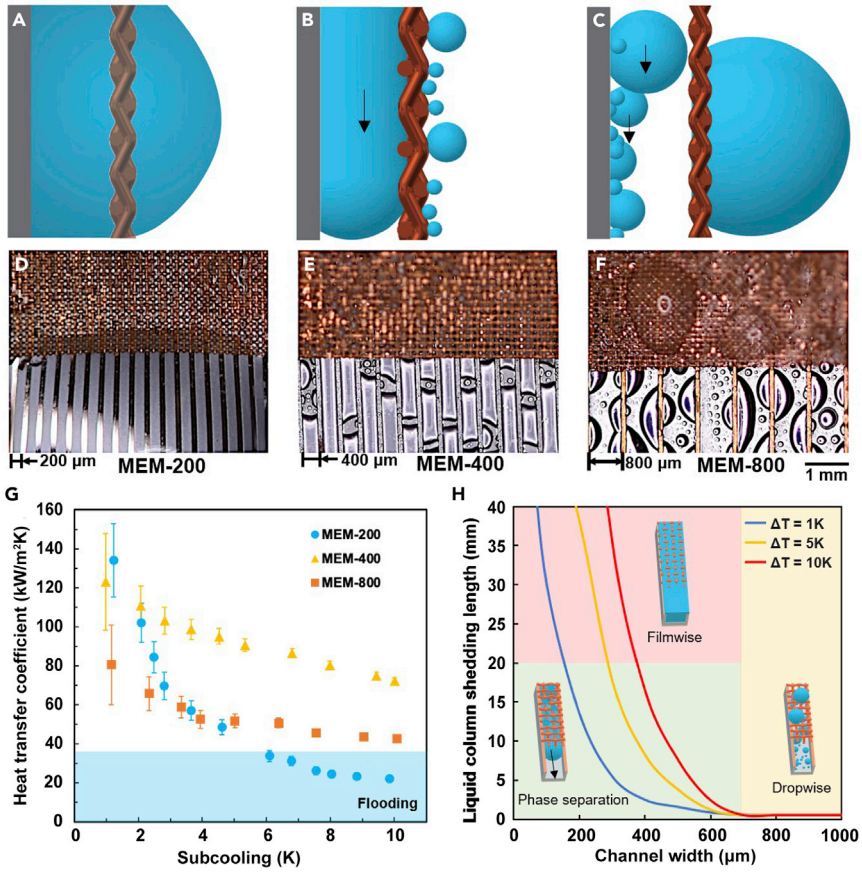

Figure 3. Phase-separation, dropwise, and filmwise condensation modes on MEM based on the widths of microchannels

(A–C) Schematics show the cross-sectional view with the condensation modes for MEM-200 (A), MEM-400 (B), and MEM-800 (C). (A) MEM-200 shows filmwise condensation due to the liquid bridge over in microchannels. (B) MEM-400 shows dropwise condensation on the hydrophobic mesh and liquid sheds off as liquid columns in microchannels. (C) MEM-800 shows discrete droplets shed off in microchannels and large droplets on the hydrophobic mesh.

(D–F) Images of the condensation behaviors for half-covered MEM-200, MEM-400, and MEM-800 at a subcooling of 5 K.

(G) Heat transfer coefficient as a function of the subcooling on MEM-200, MEM-400, and MEM-800.

(H) Critical lengths of liquid columns as a function of microchannel width at the subcooling (ΔT) of 1, 5, and 10 K, respectively. Green zone is phase separation with the highest HTC. The sample sizes are 20 mm × 20 mm.

of 72 kW/m^{2}K due to the sustainable phase separation, which is 300% larger than that of MEM-200 at an identical subcooling. In addition, MEM-400 shows up to 53% higher HTC than MEM-800. The HTC on MEM-800 is slightly higher than that on completely flooded MEM-200 at the subcooling of 10 K.

To elucidate the design rationales of the microchannels, we calculated the critical length of the liquid columns that can be spontaneously removed at varying subcooling (Figure 3H; Note S4).The liquid column in the microchannel is a cuboid geometry and the pinning force can be calculated as below:[43]

$$F_p = (2H + W_c + W_m)\gamma(\cos\theta_a - \cos\theta_r) \quad \text{(Equation 1)}$$

where F_p is the pinning force, H is the height of the microchannels, W_c is the width of the microchannels, W_m is the equivalent width of the mesh, γ is the surface tension of

Please cite this article in press as: Shan et al., Microchannel-elevated micromembrane for sustainable phase-separation condensation, Joule (2022), https://doi.org/10.1016/j.joule.2022.11.010

water, θ_a is the advancing contact angle (CA), and θ_r is the receding CA. The flow resistance is calculated by the Ergun function:[40,41]

$$\Delta P = \left(\frac{150\mu(1-\varepsilon)^2 v_s}{D_P^2 \varepsilon^3} + 1.75 \frac{1-\varepsilon}{\varepsilon^3} \frac{\rho v_s^2}{D_P} \right) L \qquad \text{(Equation 2)}$$

where ΔP is the pressure drop, L is the length of the sample, μ is the liquid viscosity, ρ is the liquid density, ε is the structure porosity, v_s is the fluid velocity, and D_p is the equivalent spherical diameter of porous media.

The detailed calculation method can be found in Figure S7, Table S2, and Note S4. As we used 20 mm × 20 mm MEM samples in the experiments, the microchannels would be flooded if the critical liquid column length is larger than 20 mm. At a subcooling of 1 K, the MEM-200 and MEM-400 have a critical length of the liquid column of 13 and 2.5 mm, respectively. This indicates that the condensate can be rapidly removed from the MEM by the gravitational force. At a subcooling of 5 K, the increased condensation rate at elevated heat flux needs a larger flow speed in the microchannels to avoid flooding, resulting in a larger flow resistance. Therefore, the critical length of the liquid column in MEM-200 increases to 38 mm, which is larger than the sample length. The microchannels of MEM-200 are fully wetted and cannot efficiently remove the condensate at this subcooling. On MEM-400, the critical length of the liquid column is 16 mm at the subcooling of 10 K, and sustainable phase separation can be achieved. As for MEM-800, the width of the microchannels is larger than 650 μm (droplet shedding diameter), so the droplets shed in each microchannel without forming elongated liquid columns and cannot achieve phase separation and dropwise condensation is observed in the microchannels. Note, the selection of channel sizes should be subject to the actual operating conditions of the system, including length scale, orientation, working fluid, and subcooling. A smaller channel size provides larger enhancement at low subcooling due to its large surface area, while a larger channel size offers a delayed transition from phase-separation condensation to flooding. To scale up MEM, the channel size could be reduced without the presence of flooding at low subcooling. However, a larger channel size provides a delayed transition from phase-separation condensation to flooding.

Accelerate liquid removal on MEM with slippery microchannels

The flow resistance of MEM can be tuned by varying the pinning forces in the microchannels. To enhance the condensation performance of MEM, we grafted a quasi-liquid coating through vapor phase grafting on the microchannels to reduce pinning forces. The quasi-liquid coating with liquid-like boundary lubrication was enabled by flexible polymer brushes with one end chemically bonded to the substrate and the other end free (see experimental procedures and Figures S8–S11 for detail). The pinning force of a droplet on a surface is characterized by CA hysteresis (CAH).[18,19] A surface with high CAH provide a larger pinning force, resulting in a larger droplet shedding diameter and slow droplet removal with the accumulation of condensate on the surface. This further results in a larger thermal resistance and hinders condensation heat transfer. We selected two coatings, silane and the QLS, for the microchannels with similar CA and different CAH. In addition, bare silicon microchannels are investigated as a control study. We used MEM-400 because it showed a sustainable high heat transfer performance with increased subcooling. Detailed fabrication processes are shown in Figures S8–S10 and Note S5. QLS and silane show comparable CA with the CAH of 1° and 9°, respectively (Figures 4A and 4B). The mobile molecule chains of QLS reduce the CAH compared with the rigid chains of silane. Figures 4C and 4D show the heat transfer performance of

Please cite this article in press as: Shan et al., Microchannel-elevated micromembrane for sustainable phase-separation condensation, Joule (2022), https://doi.org/10.1016/j.joule.2022.11.010

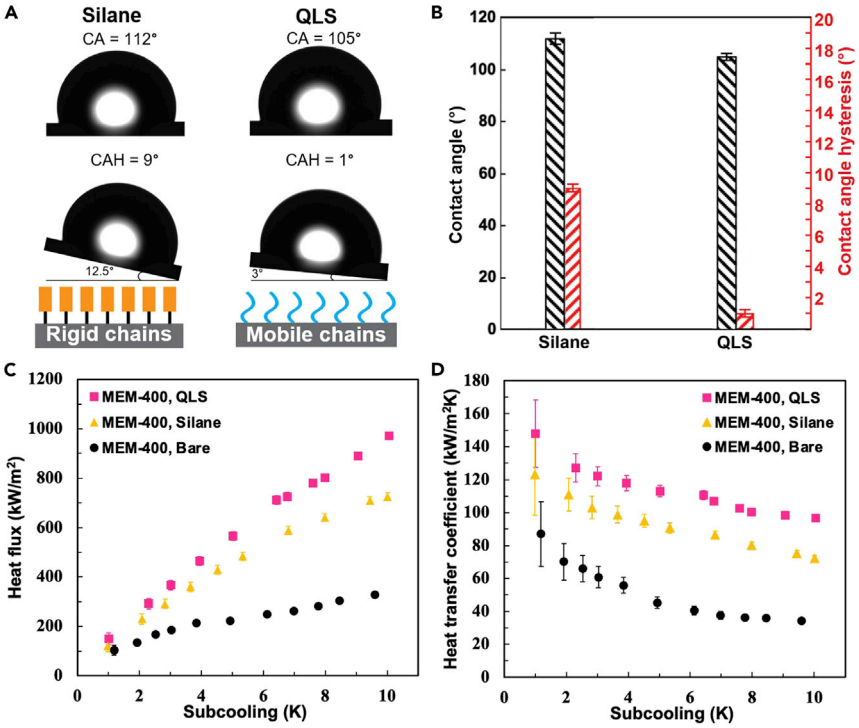

Figure 4. Slippery coatings in the microchannels provide higher performance and sustainability

(A) Images of the contact angle and contact angle hysteresis measurement of silane and QLS. Silane has a rigid polymer chain while the QLS has a mobile polymer chain.

(B) Contact angle and contact angle hysteresis for silane and QLS. Silane has a CA of 112° with a CAH of 9°. QLS shows a comparable CA of 105° with an ultra-low CAH of 1°.

(C and D) Heat flux and heat transfer coefficient curves as a function of subcooling for MEM-400 with different microchannel coatings.

the MEM with different microchannel coatings. For bare silicon channels, the HTC is 87 kW/m^{2}K at a subcooling of 1 K and it quickly decreases to 40 kW/m^{2}K at a subcooling of 6 K due to flooding. Such a low HTC is due to the fully wetted microchannels sacrificing a large area for nucleation. The significantly reduced HTC results from the large pinning force in the microchannels. For MEM-400 with QLS coated microchannel, it shows a high HTC of 147 kW/m^{2}K at a subcooling of 1 K, which is 40% larger than the MEM with bare silicon microchannel and 20% larger than the silane-coated MEM. A high HTC of 96 kW/m^{2}K is sustained at a subcooling of 10 K, which is 33% higher than the silane-coated MEM. The sustainable high HTC is due to the ultra-low CAH of the slippery QLS. The liquid column in each microchannel can shed off with a smaller length and larger speed. This leads to a faster refresh of the surface and a higher HTC. The QLS reduces the critical liquid column length in the microchannel and sustains the high HTC. Thus, CAH is one of the key factors to further enhance the heat transfer performance and sustain phase separation on MEM. The QLS coating provides a lower CAH on the microchannel surface and a higher HTC than silane. QLS has good durability in steam condensation,[14] and MEM can sustain high HTC of phase-separation condensation. Therefore, sustainable high heat transfer performance can be achieved by MEM.

MEM with two-layer meshes to further promote heat transfer

We investigated the heat transfer performance on MEM with a two-layer mesh as micromembrane (MEM-2L), which provides a large surface area for nucleation. Copper

Please cite this article in press as: Shan et al., Microchannel-elevated micromembrane for sustainable phase-separation condensation, Joule (2022), https://doi.org/10.1016/j.joule.2022.11.010

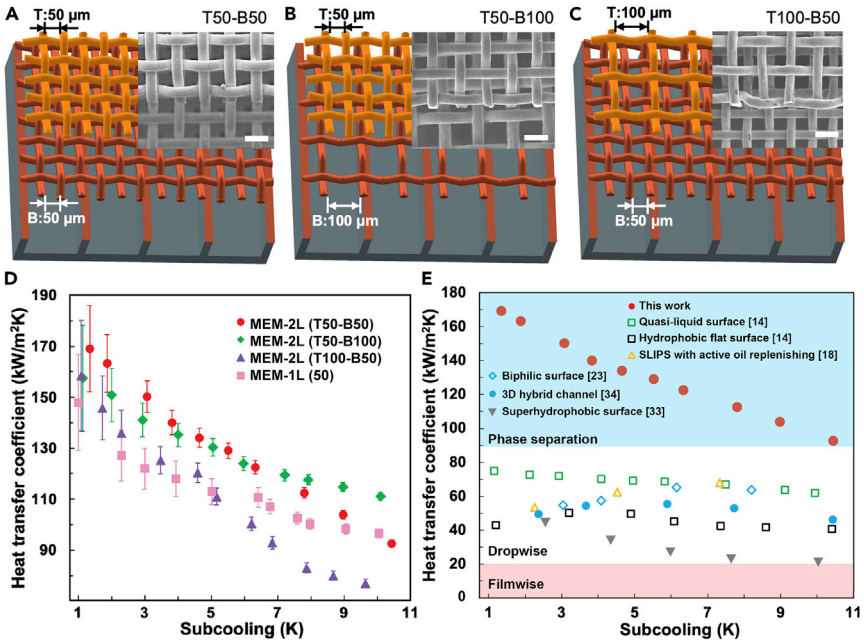

Figure 5. MEM with two-layer meshes provides a higher heat transfer coefficient

(A–C) Schematic drawings for the MEM-400 with two-layer meshes. In the schematics, the colors for the top layer mesh and the bottom layer mesh are different only for visual distinguishment. All the samples are coated with QLS. The scale bars for the inserted SEM images are 100 μm.

(D) Heat transfer coefficient curves as a function of subcooling for MEM-400 with two-layer meshes.

(E) Comparison of heat transfer coefficient between MEM and state-of-the-art surfaces.

meshes with the same wire diameter (50 μm), and different inter-mesh spacing were used. Figures 5A–5C show three different MEM with two-layer meshes that have varying inter-mesh spacing: (1) inter-mesh spacing of 50 μm for both the top and the bottom layers (i.e., T50-B50), (2) inter-mesh spacing of 50 μm for the top layer and 100 μm for the bottom layer (i.e., T50-B100), and (3) inter-mesh spacing of 100 μm for the top layer and 50 μm for the bottom layer (i.e., T100-B50). One-layer mesh MEM (MEM-1L) with an inter-mesh spacing of 50 μm is used as a baseline. The width of the microchannel is fixed as 400 μm with QLS coating to optimize the heat transfer performance. We conducted the condensation experiments on MEM-2L to characterize the HTC (Figure 5D) at varied subcoolings. At a subcooling of 1 K, the MEM-2L (T50-B50) shows the highest HTC among all samples due to its large surface area, which is 300% larger than that on a flat hydrophobic surface. MEM-2L (T100-B50) and MEM-2L (T50-B100) show comparable HTCs because their surface areas are the same. When the subcooling increases to 6 K, the HTC on MEM-2L (T100-B50) becomes lower than that on MEM-1L. MEM-2L (T50-B100) shows an HTC of 124 kW/m^{2}K, which is up to 25% higher than MEM-1L. During the droplet removal, condensed droplets on the top layer mesh are absorbed into the bottom mesh and then transported to the microchannels by direct contact with the liquid columns. At a low subcooling, the condensation rate is slow. Therefore, the flow resistance across the meshes can be neglected due to the low removal speed. However, with the increase of subcooling or heat flux, the condensation rate increases, leading to a larger mass flow rate. This results in a higher flow resistance at the bottom layer meshes. When the pore size of the bottom mesh is smaller than the top layer mesh, e.g., MEM-2L (T100-B50), the condensed liquid would be hindered by the bottom mesh due to its larger flow resistance. In contrast, when the bottom layer mesh has larger pore sizes, e.g., MEM-2L

Please cite this article in press as: Shan et al., Microchannel-elevated micromembrane for sustainable phase-separation condensation, Joule (2022), https://doi.org/10.1016/j.joule.2022.11.010

(T50-B100), the condensed liquid can be rapidly transported to the microchannels due to its smaller flow resistance, leading to a larger HTC.[5] In addition, keeping the liquid column in the Wenzel state on the bottom layer mesh is critical to remove the condensates on the top layer mesh. This allows the liquid column to reach all the small droplets on the two-layer meshes and rapidly remove them (see Figure S12 and Note S6 for detail). However, the MEM with the 50-50 mesh at the bottom makes the liquid column in the Cassie state, where droplets on the top layer mesh cannot be rapidly removed. Our results suggest that an increased inter-mesh spacing from the top to the bottom (e.g., T50-B100) can maintain each liquid column in the Wenzel state to rapidly remove droplets on the top layer mesh and increase the HTC. Compared with the state-of-the-art surfaces, our MEM can sustain phase-separation condensation at elevated subcooling of 10 K while other surfaces transit to dropwise and filmwise condensation (Figure 5E). We achieved a maximum HTC of 170 kW/m^2K, which is 300% higher than that of the dropwise condensation on a hydrophobic flat surface.

Conclusion

We report a sustainable phase separation for steam condensation on the MEM with increased subcooling. The condensed droplets are rapidly removed from the top hydrophobic micromembrane to provide a large HTC, and the liquid columns are shed off through the slippery microchannels. The top micromembrane confines the liquid columns in each microchannel. We have demonstrated that the confinement and movement of the liquid columns in microchannels are critical to achieving phase separation. Moreover, we have developed the design rationale of the microchannel geometries and used the slippery quasi-liquid coating to sustain the rapid movement of liquid columns for a high HTC. When multi-layer meshes are used, our results suggest that an increased inter-mesh spacing from the top to the bottom can reduce the flow resistance of the droplets across the mesh pores and maximize the HTC. The maximum HTC of MEM is 300% higher than that of the dropwise condensation on a hydrophobic flat surface, resulting in a 13% enhancement in overall performance for a steam heating system to save energy and cost. Unlike the prior studies that rely on hydrophilic domains, this work uses hydrophobic surfaces alone to achieve phase separation. The phase-separation condensation provides a sustainable high HTC at an elevated subcooling, which shows a paradigm to develop thermofluidic systems for water and energy applications.[8]

EXPERIMENTAL PROCEDURES

Resource availability

Lead contact

Further information and requests for resources should be directed to and will be fulfilled by the lead contact, Xianming Dai (Dai@utdallas.edu).

Materials availability

All unique structures generated in this study are available from the lead contact without restriction.

Data and code availability

All data are available from the lead contact upon reasonable request.

Methods and materials

Fabrication of microchannel-elevated micromembrane

MEMs were fabricated using photolithography, physical vapor deposition, reactive ionic etch, and electroplating. First, photolithography and physical vapor

deposition was used to form the microchannel patterns on the bare silicon wafer. Then, we performed a deep reactive ion etch (DRIE) process to form the microchannels with a depth of 200 μm. A copper mesh micromembrane was then bonded on the microchannel using electroplating at a current density of 50 mA/cm^2 for 15 min. At last, the vapor phase grafting method was used to coat silane on the MEM. The detailed fabrication process for the MEM with silane and QLS coated microchannels are shown in Figures S9–S11 and Note S5.

Steam condensation experiments

The steam condensation experiments were performed in a custom-built condensation chamber (Figure S13).[14] Steam at 100°C is generated by a steam generator and then pumped into the condensation chamber at a relative pressure of 6.9 kPa. MEM samples are vertically mounted in the condensation chamber on a copper block. Coolant at a temperature of 4°C ± 0.2°C is pumped out of a chiller (NESLAB RTE-111, Thermo Fisher Scientific) and supplied to the copper block. The mass flow rate of the coolant was adjusted to achieve the required heat flux and subcooling. Four calibrated K-type thermocouples inserted in the copper block are used to measure the heat flux, subcooling, and HTC. At last, a Nikon camera (D5600) was used to capture the condensation behavior of the MEM. Detailed experimental apparatus and measurement, and uncertainty analysis is shown in Note S7.

Contact angle measurements

A goniometer (Model 290, Rame-hart) was used to measure the apparent CA, advancing, and receding angles. The experiments were carried out at room temperature under ambient conditions. For each sample, 5 independent measurements were conducted, and the averaged values are reported in this study.

SUPPLEMENTAL INFORMATION

Supplemental information can be found online at https://doi.org/10.1016/j.joule.2022.11.010.

ACKNOWLEDGMENTS

Z.G. and X.D. acknowledge the Young Investigator Program at Army Research Office (award no. W911NF1910416). D.B. and X.D. acknowledge the National Science Foundation Faculty Early Career Development Program (award no. 2044348). L.S. was supported by the startup funds at the University of Texas at Dallas (UT Dallas). D.M. was supported by an internal grant at UT Dallas. This project was partially supported by the Office of Research at UT Dallas through the Core Facility Voucher Program.

AUTHOR CONTRIBUTIONS

X.D. conceived and supervised the research. L.S. and Z.G. contributed equally. L.S., Z.G., and X.D. designed the experiments. L.S. and Z.G. carried out the experiments. L.S., D.M., and X.D. analyzed the data. L.S., Z.G., D.M., D.B., and X.D. wrote and revised the manuscript.

DECLARATION OF INTERESTS

The authors declare no competing interests.

INCLUSION AND DIVERSITY

One or more of the authors of this paper self-identifies as an underrepresented ethnic minority in their field of research or within their geographical location.

Received: July 22, 2022
Revised: September 26, 2022
Accepted: November 21, 2022
Published: December 16, 2022

REFERENCES

1. Park, K.-C., Kim, P., Grinthal, A., He, N., Fox, D., Weaver, J.C., and Aizenberg, J. (2016). Condensation on slippery asymmetric bumps. Nature *531*, 78–82. https://doi.org/10.1038/nature16956.

2. Kim, H., Yang, S., Rao, S.R., Narayanan, S., Kapustin, E.A., Furukawa, H., Umans, A.S., Yaghi, O.M., and Wang, E.N. (2017). Water harvesting from air with metal-organic frameworks powered by natural sunlight. Science *356*, 430–434. https://doi.org/10.1126/science.aam8743.

3. Ejeian, M., and Wang, R. (2021). Adsorption-based atmospheric water harvesting. Joule *5*, 1678–1703. https://doi.org/10.1016/j.joule.2021.04.005.

4. Fujiwara, M., Takahashi, K., and Takagi, K. (2021). Improvement of condensation step of water vapor in solar desalination of seawater and the development of three-ply membrane system. Desalination *508*, 115051. https://doi.org/10.1016/j.desal.2021.115051.

5. Li, X., Wang, S., Wen, R., Ma, X., and Yang, R. (2022). Liquid film boiling enabled ultra-high conductance and high flux heat spreaders. Cell Rep. Phys. Sci. *3*, 100746. https://doi.org/10.1016/j.xcrp.2022.100746.

6. Xiong, K., Meng, L., Wang, S., and Zhang, L.W. (2022). Experimental investigation on thermal characteristics of a novel loop heat pipe for cooling high heat flux electronic chips. Int. J. Heat Mass Transf. *187*, 122569. https://doi.org/10.1016/j.ijheatmasstransfer.2022.122569.

7. Garimella, S., Milkie, J., and Macdonald, M. (2020). Condensation heat transfer and pressure drop of low-pressure hydrocarbons and synthetic refrigerants. Int. J. Heat Mass Transf. *161*, 120295. https://doi.org/10.1016/j.ijheatmasstransfer.2020.120295.

8. Derby, M.M., Adams, A.N., Chakraborty, P.P., Haque, M.R., Huber, R.A., Morrow, J.A., Riley, G.A., Ross, M., Stallbaumer, E.M., and Betz, A.R. (2020). Heat and mass transfer in the food, energy, and water nexus—a review. J. Heat Transf. *142*, 090801. https://doi.org/10.1115/1.4047089.

9. Ma, J., Sett, S., Cha, H., Yan, X., and Miljkovic, N. (2020). Recent developments, challenges, and pathways to stable dropwise condensation: a perspective. Appl. Phys. Lett. *116*, 260501. https://doi.org/10.1063/5.0011642.

10. Zhang, Y., Jia, L., Dang, C., and Qi, Z. (2022). Measurements of the liquid film thickness for annular flow during flow condensation in a circular tube. Int. J. Heat Mass Transf. *187*, 122552. https://doi.org/10.1016/j.ijheatmasstransfer.2022.122552.

11. Fang, C., David, M., Wang, F.-m., and Goodson, K.E. (2010). Influence of film thickness and cross-sectional geometry on hydrophilic microchannel condensation. Int. J. Multiphase Flow *36*, 608–619. https://doi.org/10.1016/j.ijmultiphaseflow.2010.04.005.

12. Bergman, T.L., Bergman, T.L., Incropera, F.P., Dewitt, D.P., and Lavine, A.S. (2011). Fundamentals of Heat and Mass Transfer (John Wiley & Sons).

13. Furmidge, C. (1962). Studies at phase interfaces. I. The sliding of liquid drops on solid surfaces and a theory for spray retention. J. Colloid Sci. *17*, 309–324. https://doi.org/10.1016/0095-8522(62)90011-9.

14. Monga, D., Guo, Z., Shan, L., Taba, S.A., Sarma, J., and Dai, X. (2022). Quasi-liquid surfaces for sustainable high-performance steam condensation. ACS Appl. Mater. Interfaces *14*, 13932–13941. https://doi.org/10.1021/acsami.2c00401.

15. Choi, J., Ludwig, P., and Brand, L. (2013). Steam system balancing and tuning for multifamily residential buildings in Chicagoland-second year of data collection. National Renewable Energy Lab (NREL). https://www.nrel.gov/docs/fy13osti/60003.pdf.

16. Lewis, G.N., Randall, M., Pitzer, K.S., and Brewer, L. (2020). Thermodynamics (Courier Dover Publications).

17. ASHRAE (1993). ASHRAE Handbook: Fundamentals (ASHRAE).

18. Seo, D., Shim, J., Lee, C., and Nam, Y. (2020). Brushed lubricant-impregnated surfaces (BLIS) for long-lasting high condensation heat transfer. Sci. Rep. *10*, 2959. https://doi.org/10.1038/s41598-020-59683-z.

19. Bai, H., Wang, L., Ju, J., Sun, R., Zheng, Y., and Jiang, L. (2014). Efficient water collection on integrative bioinspired surfaces with star-shaped wettability patterns. Adv. Mater. *26*, 5025–5030. https://doi.org/10.1002/adma.201400262.

20. Hou, Y., Yu, M., Chen, X., Wang, Z., and Yao, S. (2015). Recurrent filmwise and dropwise condensation on a beetle mimetic surface. ACS Nano *9*, 71–81. https://doi.org/10.1021/nn505716b.

21. Mahapatra, P.S., Ghosh, A., Ganguly, R., and Megaridis, C.M. (2016). Key design and operating parameters for enhancing dropwise condensation through wettability patterning. Int. J. Heat Mass Transf. *92*, 877–883. https://doi.org/10.1016/j.ijheatmasstransfer.2015.08.106.

22. Orejon, D., Shardt, O., Waghmare, P.R., Gunda, N.S.K., Takata, Y., and Mitra, S.K. (2016). Droplet migration during condensation on chemically patterned micropillars. RSC Adv. *6*, 36698–36704. https://doi.org/10.1039/C6RA03862J.

23. Egab, K., Alwazzan, M., Peng, B., Oudah, S.K., Guo, Z., Dai, X., Khan, J., and Li, C. (2020). Enhancing filmwise and dropwise condensation using a hybrid wettability contrast mechanism: circular patterns. Int. J. Heat Mass Transf. *154*, 119640. https://doi.org/10.1016/j.ijheatmasstransfer.2020.119640.

24. Bintein, P.-B., Lhuissier, H., Mongruel, A., Royon, L., and Beysens, D. (2019). Grooves accelerate dew shedding. Phys. Rev. Lett. *122*, 098005. https://doi.org/10.1103/PhysRevLett.122.098005.

25. Peng, B., Ma, X., Lan, Z., Xu, W., and Wen, R. (2014). Analysis of condensation heat transfer enhancement with dropwise-filmwise hybrid surface: droplet sizes effect. Int. J. Heat Mass Transf. *77*, 785–794. https://doi.org/10.1016/j.ijheatmasstransfer.2014.05.052.

26. Chaudhury, M.K., Chakrabarti, A., and Tibrewal, T. (2014). Coalescence of drops near a hydrophilic boundary leads to long range directed motion. Extreme Mech. Lett. *1*, 104–113. https://doi.org/10.1016/j.eml.2014.11.007.

27. Narhe, R.D., and Beysens, D.A. (2004). Nucleation and growth on a superhydrophobic grooved surface. Phys. Rev. Lett. *93*, 076103. https://doi.org/10.1103/PhysRevLett.93.076103.

28. Miljkovic, N., Enright, R., Nam, Y., Lopez, K., Dou, N., Sack, J., and Wang, E.N. (2013). Jumping-droplet-enhanced condensation on scalable superhydrophobic nanostructured surfaces. Nano Lett. *13*, 179–187. https://doi.org/10.1021/nl303835d.

29. Chen, X., Patel, R.S., Weibel, J.A., and Garimella, S.V. (2016). Coalescence-induced jumping of multiple condensate droplets on hierarchical superhydrophobic surfaces. Sci. Rep. *6*, 18649. https://doi.org/10.1038/srep18649.

30. Boreyko, J.B., and Chen, C.-H. (2009). Self-propelled dropwise condensate on superhydrophobic surfaces. Phys. Rev. Lett.

103, 184501. https://doi.org/10.1103/PhysRevLett.103.184501.

31. Mukherjee, R., Berrier, A.S., Murphy, K.R., Vieitez, J.R., and Boreyko, J.B. (2019). How surface orientation affects jumping-droplet condensation. Joule *3*, 1360–1376. https://doi.org/10.1016/j.joule.2019.03.004.

32. Cha, H., Vahabi, H., Wu, A., Chavan, S., Kim, M.-K., Sett, S., Bosch, S.A., Wang, W., Kota, A.K., and Miljkovic, N. (2020). Dropwise condensation on solid hydrophilic surfaces. Sci. Adv. *6*, eaax0746. https://doi.org/10.1126/sciadv.aax0746.

33. Wen, R., Xu, S., Ma, X., Lee, Y.-C., and Yang, R. (2018). Three-dimensional superhydrophobic nanowire networks for enhancing condensation heat transfer. Joule *2*, 269–279. https://doi.org/10.1016/j.joule.2017.11.010.

34. Lo, C.-W., Chu, Y.-C., Yen, M.-H., and Lu, M.-C. (2019). Enhancing condensation heat transfer on three-dimensional hybrid surfaces. Joule *3*, 2806–2823. https://doi.org/10.1016/j.joule.2019.08.005.

35. Lee, J.H., Jung, B., Park, G.-s., and Kim, H.-Y. (2022). Condensation and wicking of water on solid nanopatterns. Phys. Rev. Fluids *7*, 024202. https://doi.org/10.1103/PhysRevFluids.7.02420.

36. Oh, J., Zhang, R., Shetty, P.P., Krogstad, J.A., Braun, P.V., and Miljkovic, N. (2018). Thin film condensation on nanostructured surfaces. Adv. Funct. Mater. *28*, 1707000. https://doi.org/10.1002/adfm.201707000.

37. Winter, R.L., Ölçeroğlu, E., Chen, Z., Lau, K.K.S., and McCarthy, M. (2021). Formation and stability of thin condensing films on structured amphiphilic surfaces. Langmuir *37*, 2683–2692. https://doi.org/10.1021/acs.langmuir.0c03252.

38. Cheng, Y., Wang, M., Sun, J., Liu, M., Du, B., Liu, Y., Jin, Y., Wen, R., Lan, Z., Zhou, X., et al. (2021). Rapid and persistent suction condensation on hydrophilic surfaces for high-efficiency water collection. Nano Lett. *21*, 7411–7418. https://doi.org/10.1021/acs.nanolett.1c01928.

39. Wen, R., Xu, S., Zhao, D., Yang, L., Ma, X., Liu, W., Lee, Y.-C., and Yang, R. (2018). Sustaining enhanced condensation on hierarchical mesh-covered surfaces. Natl. Sci. Rev. *5*, 878–887. https://doi.org/10.1093/nsr/nwy098.

40. Ergun, S. (1952). Fluid flow through packed columns. Chem. Eng. Prog. *48*, 89–94. https://doi.org/10.1021/ie50474a011.

41. Dai, X., Yang, F., Yang, R., Lee, Y.-C., and Li, C. (2013). Micromembrane-enhanced capillary evaporation. Int. J. Heat Mass Transf. *64*, 1101–1108. https://doi.org/10.1016/j.ijheatmasstransfer.2013.05.030.

42. Dai, X., Yang, F., Yang, R., Huang, X., Rigdon, W.A., Li, X., and Li, C. (2014). Biphilic nanoporous surfaces enabled exceptional drag reduction and capillary evaporation enhancement. Appl. Phys. Lett. *105*, 191611. https://doi.org/10.1063/1.4901962.

43. Quéré, D. (2008). Wetting and roughness. Annu. Rev. Mater. Res. *38*, 71–99. https://doi.org/10.1146/annurev.matsci.38.060407.132434.